Tuning Squeeze-film Damping in an Air-coupled Electrostatic Ultrasonic Transducer by a Structured Cavity

Franziska Wall[1], Hermann A.G. Schenk[2], Anton Melnikov[2], Marcel Jongmanns[3], Jorge M. Monsalve[3]

[1] *Fraunhofer Institut für Photonische Mikrosysteme IPMS, 01109 Dresden, Deutschland, Email: franziska.wall@ipms.fraunhofer.de*

[2] *Bosch Sensortec GmbH, 01109 Dresden, Deutschland*

[1] *Fraunhofer Institut für Photonische Mikrosysteme IPMS, 01109 Dresden, Deutschland*

Introduction

Lateral electrostatically driven actuators enable air-coupled ultrasound transducers (L-cMUTs [1]) with resonance frequencies in the kHz range, targeting low absorption losses in free-field. The CMOS-compatible device, driven with low voltages, allows a broadband response. Distance measurements by e.g. time-of-flight evaluations have applications in robotics and automation and enable gesture recognition [2], which in turn can be used for augmented and virtual reality solutions. Another area of application is ultrasound imaging, which is used for non-contact, non-destructive topology analysis, for example, or predictive maintenance by vibration analysis [3]. Further, flow measurements allow the detection of hydrogen in natural gas [4] or medical applications such as spirometry. In contrast to piezoelectric (pMUTs) and membrane-based, capacitive transducers (cMUTs), they utilize the chip volume pointing towards higher sound pressure levels per area. A periodic volume change caused by the actuator movement in an acoustic cavity generates the sound signal (fig. 1). Within one device multiple actuators work together. The L-cMUT can be used as a transmitter as well as a receiver and chips can be relatively easy divided into subgroups [1].

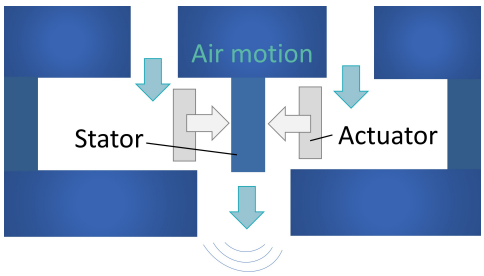

Figure 1: Schematic side-view of the L-cMUT actuator

Figure 2 is a schematic top view of the actuator's geometry with a stator structured by the beam's first bending mode $\psi_0(\xi)$.

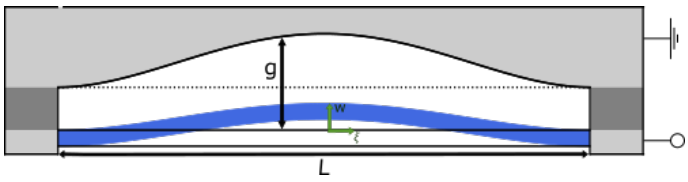

Figure 2: Schematic top-view of a microbeam driven by a structured stator

The smaller the distance between the actuator and the stator electrode, the stronger the driving force. Contrary, the squeeze-film damping increases with smaller distances. High damping restricts the frequency range, while low damping can lead to resonances and instabilities. The damping force that occurs depends on the natural mode under consideration [5] and the working point [6]. Further, the actuator geometry may vary the air thickness and thereby the damping as for e.g. curved beams [7] or tips used in atomic force microscopy [8]. Finite-element-method (FEM) simulations including various working points as well as geometries can become time consuming. Thus, a order-reduced modeling approach for the L-cMUT is desirable. As shown experimentally in [9] and evaluated analytically in [10] an electrostatically driven beam can be modeled with a 1-DOF equation. Thereby, the prismatic actuator's bending profile $w(\tau, \xi)$, as a function of the time τ and the position along the beam ξ, is described by the dimensionless Euler-Bernoulli-beam equation [11]

$$\frac{\partial^2 w(\tau,\xi)}{\partial \tau^2} + c\frac{\partial w(\tau,\xi)}{\partial \tau} + \frac{\partial^4 w(\tau,\xi)}{\partial \xi^4} = (\gamma + N)\frac{\partial^2 w(\tau,\xi)}{\partial \xi^2} + \alpha_2 \frac{v(\tau)^2}{(1-w(\tau,\xi))^2} \tag{1}$$

with the axial tensile force N as well as the damping coefficient c,

$$\alpha_1 = 6\left(\frac{g_0}{t}\right)^2 \ , \ \alpha_2 = \frac{6\epsilon l^4}{t^3 g_0^3} \tag{2}$$

and

$$\gamma = \alpha_1 \int_{-\frac{1}{2}}^{+\frac{1}{2}} \left(\frac{\partial w(\tau,\zeta)}{\partial \zeta}\right)^2 \mathrm{d}\zeta \tag{3}$$

with the dielectric constant ϵ. Here the beam geometry is chosen by the beam length $l = 1000\,\mu m$, the thickness $t = 3\,\mu m$, the width $h = 75\,\mu m$, the initial gap $g_0 = 10\,\mu m$ similar to [9] and [12]. The dimensionless voltage u is related to the physical voltage v by

$$u = \psi_0(0) \cdot \alpha_2 \cdot v \tag{4}$$

with $\psi_0(0) \approx 1.588$. Where $\psi_0(\xi)$ refers to the undamped, clamped-clamped beam's first bending mode with $\beta_0 \approx 4.73$ for $\xi \in [-0.5, 0.5]$,

$$\psi_0(\xi) = \frac{\cosh(\beta_0 \cdot \xi)}{\cosh(\frac{\beta_0}{2})} - \frac{\cos(\beta_0 \cdot \xi)}{\cos(\frac{\beta_0}{2})}. \tag{5}$$

An efficient 1-DOF model can be constructed by a single-mode approximation, assuming

$$w(\xi,\tau) \approx z(\tau)\ \frac{\psi_0(\xi)}{\psi_0(0)}. \tag{6}$$

Schenk et al. developed in [10] a precise evaluation of the electrostatic force within this approximation for the Coulomb integral. By shifting the variable z a stator electrode structured by ψ_0 can be modelled [1]. Recently, this approach was extended to include the squeeze-film damping for this type of structured stator [12]. As observed in other MEMS structures [13], the single-mode approximation results in a precise lumped element model (LPM). By structuring the stator not only the driving force but also the damping can be tuned. Here, we briefly summarize the model with a straight stator as well as a structured stator. The single-mode approach is further numerically evaluated for other stator geometries and compared with modal FEM-simulations. This indicates the applicability of the single-mode model also for other stator geometries that are similar to the first bending mode and is a basis for the optimization of the squeeze-film damping, an important design parameter with regard to broadband applications.

Squeeze-film damping by a straight stator

According to [14], the squeeze-film damping is here modelled by the Reynolds equation for the pressure p

$$\frac{\partial}{\partial x}\left(H^3 p\frac{\partial p}{\partial x}\right)+\frac{\partial}{\partial y}\left(H^3 p\frac{\partial p}{\partial y}\right)= 12\mu_{\text{eff}}\left(H\frac{\partial p}{\partial t}+p\frac{\partial H}{\partial t}\right) \tag{7}$$

with the viscosity μ and the air thickness H. The clearance above the actuator is neglected and three closed boundaries with zero pressure are combined with one open edge with ambient pressure [15]. For the geometry under consideration, the pressure variation along the beam can be neglected [13]. The damping force per unit length becomes

$$F_{SQ}=\int_{-h/2}^{h/2} 6\mu_{\text{eff}}\left(-\frac{3}{4}h^2+hy+y^2\right)\left(\frac{1}{g^3}\frac{\partial \hat{w}}{\partial t}\right)\mathrm{d}y = -\frac{4t^3\mu_{\text{eff}}}{g^3}\frac{\partial \hat{w}}{\partial t}. \tag{8}$$

The dimensionless damping coefficient is [11]

$$c_{SQ}=4\frac{t^3\mu_{\text{eff}}}{g^3}\frac{l^2}{\sqrt{th\rho c}}. \tag{9}$$

Compared to the result for a strip plate in [16] the coefficient differs by a factor due to the pressure boundary conditions [15]. Further, the damping ration ζ_{SQ} includes the actuator's mechanical resonance frequency ω_0,

$$\zeta_{SQ}=\frac{c_{\text{SQ}}}{2m\omega_0}=4\sqrt{3}\frac{\mu_{\text{eff}}}{\sqrt{\rho\mathcal{E}\lambda_0}}\frac{h^2l^2}{t^2}\frac{1}{g^3}. \tag{10}$$

Damping by a structured stator

Both, the beam deflection $w(\xi)$ as well as the structured stator $s(\xi)$ results in a position dependent air thickness $g(x)$, which becomes compared to the gap without both effects g_0, the dimensionless film thickness d,

$$d(\xi,w)=\frac{g(x)}{g_0}=1+s(\xi)-w(\xi). \tag{11}$$

Within the single-mode approximation (eq. 6) the squeeze-film force (eq. 8) is proportional to the integral $df_0(s,z)$,

$$df_0(s,z)=2\int_{-0.5}^{0.5}\frac{1}{\left(1+s(\xi)-z\frac{\psi_0(\xi)}{\psi_0(0)}\right)^3}\cdot\left(\frac{\psi_0(\xi)}{\psi_0(0)}\right)^2\mathrm{d}\xi. \tag{12}$$

Thus, the damping coefficient with a structured stator $c_{SQ}(s)$ is connected to the damping coefficient without a structuring $c_{SQ}(0)$ (eq. 9) by

$$c_{SQ}(s)=\frac{df_0(s)}{df_0(0)}\cdot c_{SQ}(0) \tag{13}$$

Similarly, the damping ratio of with a structured cavity $\zeta_{SQ}(s)$ is related to the straight cavity (eq. 10) by

$$\zeta_{SQ}(s)=\frac{df_0(s)}{df_0(0)}\cdot \zeta_{SQ}(0). \tag{14}$$

Note, algebraic equations for the integral 12 with a stator structured with $s(\xi)\sim\psi_0(\xi)$ are presented in [12].

Results for a structured stator

Here, we evaluate the integral df_0 (eq. 12) numerically for different stator geometries. Exemplary, we consider stator geometries similar to the first bending mode of the type

$$s_n(\xi)=s_0\cdot\left(\frac{\psi_0(\xi)}{\psi_0(0)}\right)^n \tag{15}$$

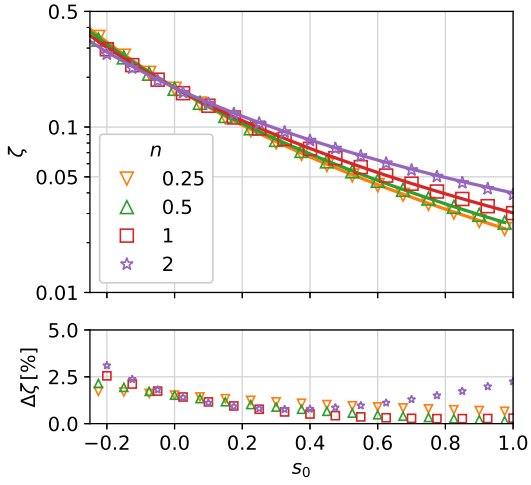

Figure 3: Damping coefficient of different geometries proportional to ψ_0^n (eq. 15) by a 3D modal FEM simulation (markers) compared to a numerical evaluation of eq. 8 as well as the relative deviation $\Delta\zeta$ between them

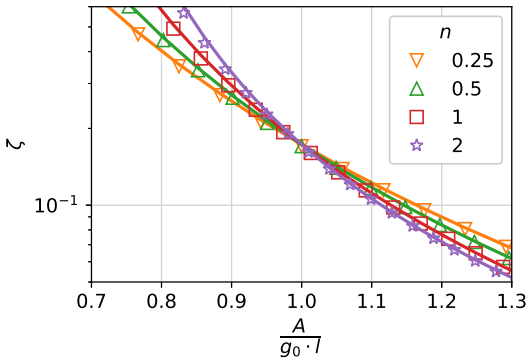

Figure 4: Damping coefficient (fig.3) of different geometries proportional to ψ_0^n (eq. 15) as a function of the cavity area

with a scaling factor s_0 determining the maximal fluid thickness and different powers n. Additionally, we evaluate higher bending modes $\psi_m(\xi)$ as stator structures

$$s_m(\xi) = s_0 \cdot \left(\frac{\psi_m(\xi)}{\psi_m(0)} \right). \tag{16}$$

These numerical predictions for $\zeta_{\mathrm{SQ}}(s)$ (eq. 14 with eq. 8 and 10) are compared with a 3D-modal FEM simulation in COMSOL multiphysics like in [15] which considers the mechanical and fluid domain. The fluid damping is included with thin-film nodes by the full Reynolds equation. The damping coefficient is reproduced precisely for stators similar to the first bending mode (fig. 3). Further, cavities with the same area result in different damping coefficients depending on the stator's geometry (fig. 4). Figure 5 displays the damping coefficient for different recess sizes as well as shorter beams for equation 15 with n=2. This indicates the applicability of the modeling over a wide geometry range. However, the single-mode approximation becomes less precise with stator structures including additional local extrema like higher bending modes ψ_m. Only the qualitative dependency of the damping coefficient towards a scaling of the stator structure is reproduced (fig. 6).

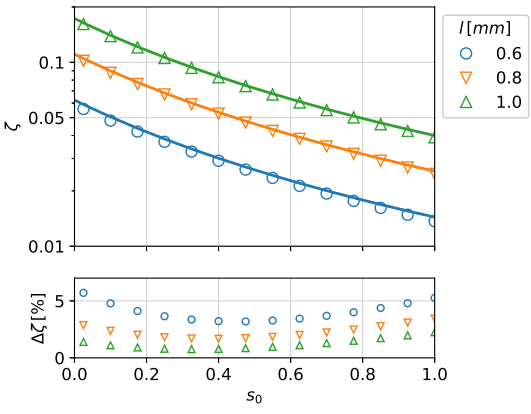

Figure 5: Damping coefficient with $n = 2$ (eq. 15) for different beam length by a 3D modal FEM simulation (markers) compared to a numerical evaluation of eq. 8

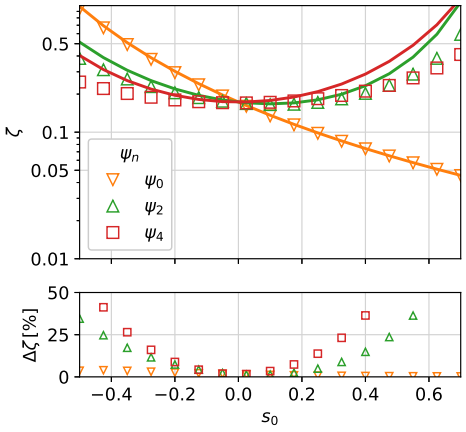

Figure 6: Damping coefficient of different geometries proportional to the beam bending modes ψ_m (eq. 16) by a 3D modal FEM simulation (markers) compared to a numerical evaluation of eq. 8

Discussion

The essential assumption is the validity of the zero-mode approximation (eq. 12). Thereby, ψ_0 should not only be dominant for the bending profile with electrostatic drive, but also for the damped eigenmodes. From a mechanical point of view, the energetic distance between the eigenmodes should be large to ensure that ψ_0 is the dominant mode [9]. Further, the spatial distribution of the driving as well as damping force may vary the dominant mode shape. Here, stator shapes that are similar to ψ_0 can be precisely modelled by the single-mode approximation. This may enable e.g. an effective investigation of manufacturing tolerances. In the future, stator geometries with additional local extrema will require further development of the modeling for a quantitative prediction. Very thin beams might need a treatment with the Timoshenko beam equation instead of the Euler-Bernoulli beam equation [9]. Moreover, high aspect ratios by e.g. short beams may lead to a plate-like system. For those the impact of the the pressure boundary conditions and the coupling towards the beam motion gets more significant [17]. With a look at the application as an ultrasonic transducer smaller gaps promise higher driving forces. Smaller gaps ($\lessapprox 7\mu m$) need a model extension, because the continuum assumption for the Reynolds equation is no longer fullfilled. An effective viscosity [18], which might be due to the structured gap also position depended [19], might be necessary to model the slip flow. Additionally, smaller gaps combined with high frequencies lead to higher squeeze numbers making a compressible model necessary [16]. Moreover, various optimization goals appear within the context of L-cMUTs. For instance, the pull-in voltage should be large. If higher voltages are applied, the electrodes will touch and the device may be destroyed by the short circuit. Additionally, small driving voltages with a high sensitivity of the response are desirable to ensure a low power consumption. Further, the pitch between actuator units should be small to maximize the sound pressure level per area in order to reach cost efficient small devices. High damping might

limit the frequency range by the low-pass behaviour and larger damping might lead to resonances which hinder broadband response.

Conclusion

The geometric shape of the stator electrode gives an additional possibility to tune the squeeze-film damping of L-cMUT's. Not only the cavity's volume but also its geometric shape plays a decisive role for the damping. The single-mode approximation allows a numerical estimation of the damping coefficient for a stator structures similar to the beam's first bending mode.

References

[1] J. M. Monsalve, A. Melnikov, M. Stolz, A. Mrosk, M. Jongmanns, F. Wall, S. Langa, I. Marica-Bercu, T. Brändel, M. Kircher, *et al.*, "Proof of concept of an air-coupled electrostatic ultrasonic transducer based on lateral motion," *Sensors and Actuators A: Physical*, vol. 345, p. 113813, 2022.

[2] J. M. M. Guaracao, M. Kircher, F. Wall, M. Krenkel, B. Kaiser, S. Langa, and H. Schenk, "First time of nanoscopic electrostatic drives pushing for ultrasonic transmission for gesture recognition," in *2020 IEEE International Ultrasonics Symposium (IUS)*, pp. 1–4, IEEE, 2020.

[3] P. Suawa, A. Halbinger, M. Jongmanns, and M. Reichenbach, "Noise-robust machine learning models for predictive maintenance applications," *IEEE Sensors Journal*, 2023.

[4] J. Monsalve, J. Amelung, B. Betz, S. Koch, C. Ruffert, U. Völz, M. Jongmanns, and M. Wiersig, "A5. 4-rapid characterisation of mixtures of hydrogen and natural gas by means of ultrasonic time-delay estimation," *Lectures*, pp. 67–68, 2023.

[5] N. Alcheikh, L. Kosuru, N. Jaber, M. Bellaredj, and M. I. Younis, "Influence of squeeze film damping on the higher-order modes of clamped–clamped microbeams," *Journal of Micromechanics and Microengineering*, vol. 26, no. 6, p. 065014, 2016.

[6] D. Van Hieu, L. Van Tam, K. Hane, and C. M. Hoang, "Models for analyzing squeeze film air damping depending on oscillation modes of micro/nano beam resonators," *Archive of Applied Mechanics*, vol. 91, no. 1, pp. 363–373, 2021.

[7] H. M. Ouakad, H. M. Al-Qahtani, and M. A. Hawwa, "Influence of squeeze-film damping on the dynamic behavior of a curved micro-beam," *Advances in mechanical engineering*, vol. 8, no. 6, p. 1687814016650120, 2016.

[8] Z. Wei, J. Liu, X. Zheng, Y. Sun, and R. Wei, "Influence of squeeze film damping on quality factor in tapping mode atomic force microscope," *Journal of Sound and Vibration*, vol. 491, p. 115720, 2021.

[9] A. Melnikov, H. A. Schenk, J. M. Monsalve, F. Wall, M. Stolz, A. Mrosk, S. Langa, and B. Kaiser, "Coulomb-actuated microbeams revisited: experimental and numerical modal decomposition of the saddle-node bifurcation," *Microsystems & Nanoengineering*, vol. 7, no. 1, p. 41, 2021.

[10] H. A. Schenk, A. Melnikov, F. Wall, M. Gaudet, M. Stolz, D. Schuffenhauer, and B. Kaiser, "Electrically actuated microbeams: An explicit calculation of the coulomb integral in the entire stable and unstable regimes using a chebyshev-edgeworth approach," *Physical Review Applied*, vol. 18, no. 1, p. 014059, 2022.

[11] A. H. Nayfeh, M. I. Younis, and E. M. Abdel-Rahman, "Dynamic pull-in phenomenon in mems resonators," *Nonlinear dynamics*, vol. 48, pp. 153–163, 2007.

[12] F. Wall, H. A. G. Schenk, A. Melnikov, and J. M. Monsalve Guaracao, "Squeeze film damping by a structured cavity in an air-coupled electrostatic ultrasonic transducer." 29th International Congress on Sound and Vibration.

[13] S. Krylov and R. Maimon, "Pull-in dynamics of an elastic beam actuated by continuously distributed electrostatic force," *J. Vib. Acoust.*, vol. 126, no. 3, pp. 332–342, 2004.

[14] M. I. Younis, *MEMS linear and nonlinear statics and dynamics*, vol. 20. Springer Science & Business Media, 2011.

[15] A. Melnikov, H. A. Schenk, F. Wall, J. M. Monsalve, L. Ehrig, M. Stolz, A. Mrosk, S. Langa, and B. Kaiser, "Squeeze film damping in mems loudspeakers: analysis of a clamped-clamped microbeam," in *Microfluidics, BioMEMS, and Medical Microsystems XX*, vol. 11955, pp. 13–19, SPIE, 2022.

[16] M. Bao and H. Yang, "Squeeze film air damping in mems," *Sensors and Actuators A: Physical*, vol. 136, no. 1, pp. 3–27, 2007.

[17] A. H. Nayfeh and M. I. Younis, "A new approach to the modeling and simulation of flexible microstructures under the effect of squeeze-film damping," *Journal of Micromechanics and Microengineering*, vol. 14, no. 2, p. 170, 2003.

[18] T. Veijola, H. Kuisma, J. Lahdenperä, and T. Ryhänen, "Equivalent-circuit model of the squeezed gas film in a silicon accelerometer," *Sensors and Actuators A: Physical*, vol. 48, no. 3, pp. 239–248, 1995.

[19] H. M. Ouakad, H. M. Al-Qahtani, and M. A. Hawwa, "Influence of squeeze-film damping on the dynamic behavior of a curved micro-beam," *Advances in mechanical engineering*, vol. 8, no. 6, p. 1687814016650120, 2016.